[2] Reinecke, W. G. and Waldman, G. D., "Particle Trajectories, Heating, and Breakup in Hypersonic Shock Layers," AIAA Paper 69-712, San Francisco, 1969.

[3] Probstein, R. F. and Fassio, F., "Dusty Hypersonic Flows," *AIAA Journal*, Vol. 8, No. 4, April 1970, pp. 772–779.

[4] Nicholson, J., "Drop Breakup by Airstream Impact," *Rain Erosion and Associated Phenomena*, Rept. N68-19401-427, 1967, Royal Aircraft Establishment, Farnborough, England, pp. 342–369.

[5] Ranger, A. and Nicholls, J., "Aerodynamic Shattering of Liquid Drops," *AIAA Journal*, Vol. 7, No. 2, Feb. 1969, pp. 285–290.

[6] Inouye, M., "Shock Standoff Distance For Equilibrium Flow Around Hemispheres Obtained From Numerical Calculations," *AIAA Journal*, Vol. 3, No. 1, Jan. 1965, p. 172.

[7] Seiff, A., "Recent Information on Hypersonic Flow Fields," *Gasdynamics in Space Exploration*, SP-24, NASA, 1962.

[8] Lees, L., "Laminar Heat Transfer over Blunt-Nosed Bodies at Hypersonic Flight Speeds," *Jet Propulsion*, Vol. 26, April 1956, p. 259.

[9] Rose, P. H. and Stark, W. J., "Stagnation Point Heat Transfer Measurements in Dissociated Air," *Journal of the Aerospace Sciences*, Vol. 25, Feb. 1958, p. 86.

[10] Reinecke, W. G. and McKay, W. L., "Experiments on Water Drop Breakup Behind Mach 3 to 12 Shocks," AVATD-0172-69-RR, June 1969, Avco Corp., Wilmington, Mass.

[11] Reinecke, W. G. and Waldman, G. D., "An Investigation of Water Drop Disintegration in the Region Behind Strong Shock Waves," 3rd International Conference on Rain Erosion and Related Phenomena, Hampshire, England, Aug. 1970.

[12] Shanks, D., "Non-linear Transformations of Divergent and Slowly Convergent Sequences," *Journal of Mathematics and Physics*, Vol. 34, 1955, pp. 1–42.

JUNE 1971 AIAA JOURNAL VOL. 9, NO. 6

A Unified Analysis of Gaseous Jet Penetration

F. S. Billig,* R. C. Orth,† and M. Lasky‡
The Johns Hopkins University, Applied Physics Lab., Silver Spring, Md.

The strengths and weaknesses of various physical and mathematical concepts that have been employed in the development of theories concerning transverse gaseous jet penetration into a supersonic stream are discussed in relation to the latest experimental results reported in the literature. A new unified model that provides excellent agreement with measured flow field properties is presented. The development of this model rests on the similarity that exists between a jet discharging into a quiescent medium and a jet discharging into crossflow. By the suitable definition of an "effective back pressure," a correlation is obtained between the normal distance to the center of the Mach disk and the ratio of injection pressure to effective back pressure. Other correlations are used to obtain the size and shape of the initial portion of the jet, which permit the calculation of a) the complete trajectory of the injectant and b) a one-dimensional approximation of the mass-averaged properties at any point along the trajectory downstream of the Mach disk.

Nomenclature

A = area
A_p = projected area
C_p = pressure coefficient = $(p - p_a)/q_a$
C_p^* = stagnation pressure coefficient defined by Eq. (6b)
D = jet diameter
D_j^* = diameter of jet orifice at sonic point
F_N = normal force on jet element (Fig. 8)
F_x = defined as $\int_{A_x} p dA$
h = enthalpy [Eq. (4)]
h = radius of quarter sphere-half cylinder injection model
h' = diameter of spherical nosed cylinder injection model
$\tilde{h}$ = ordinate of jet center of mass
K = constant defined in Eq. (42)
m = mass
M = Mach number
p = pressure
p_{eb} = effective back pressure = $\frac{2}{3}p_{t'a}$
p_t' = pitot pressure
p_j^* = pressure at sonic point in jet orifice
q = dynamic pressure = $\rho u^2/2$
r = jet radius
R_c = local radius of curvature for jet trajectory
s = distance along jet trajectory
T = temperature
u = velocity
W = Mach disk diameter (Fig. 8)
x = axial distance measured from center of injection port
y = normal distance from point of injection
y_1 = normal distance to center of Mach disk (Fig. 4)
$\bar{y}$ = maximum ordinate of Mach disk (Fig. 8)
z = lateral distance measured from center of injection port
α = local angle of freestream flow (Fig. 1)
$\hat{\alpha}$ = defined in Eq. (27) (Fig. 8)
δ = local angle of jet centerline (Fig. 1)
$\hat{\delta}$ = local angle of jet surface in plane of symmetry
Γ = function defined by Eq. (12b)
γ = ratio of specific heats

Superscript

$(\bar{\ })$ = averaged one-dimensional property at a particular station

Subscripts

a = undisturbed freestream conditions at upstream edge of control volume (Fig. 1)
b = freestream conditions at downstream edge of control volume (Fig. 1)
c = jet stream conditions at downstream edge of control volume (Fig. 1)
j = jet conditions at point of injection (Fig. 1)
j_1 = jet diameter for $p_{tj}/p_{ta} = 1$ (Fig. 11)
A_x = axial direction of surface integration on jet-freestream boundary (Fig. 1)

Presented as Paper 70-93 at the AIAA 8th Aerospace Sciences Meeting, New York, January 19–21, 1970; submitted August 11, 1970; revision received December 14, 1970. This work was supported by NASA Office of Aeronautical Research, Advanced Research and Technology under Contract N00017-62-C-0604 with the Department of the Navy.

* Supervisor Hypersonic Ramjets Project. Associate Fellow AIAA.
† Engineer, Hypersonic Ramjets Project.
‡ Associate Mathematician, Hypersonic Ramjets Project.

CB = normal direction of surface integration on control boundary (Fig. 1)
N = normal direction of surface integration on jet-freestream boundary (Fig. 1)
WP = normal direction of surface integration on freestream-wall boundary (Fig. 1)
WS = normal direction of surface integration on jet-wall boundary (Fig. 1)
t = total conditions
∞ = ambient conditions in a quiescent medium
1 = conditions ahead of the Mach disk (Fig. 8)
2 = conditions aft of the Mach disk (Fig. 8)
3 = conditions at point where jet pressure drops to p_a (Fig. 8)

Introduction

DURING the past several years considerable attention has been given to the problem of the interaction caused by the transverse injection of a gas into a supersonic stream. The earlier work was concerned with alteration of the surface pressure field to produce desired aerodynamic forces, e.g., thrust vector control in rocket nozzles. More recently, fuel injection into a supersonic combustion ramjet (scramjet) has been of principal interest. Whereas in the former case, very general approximations of the flowfield yield adequate estimates for the side force,[1–5] a much more rigorous description of the interaction zone must be given to obtain a realistic definition of the mass distribution in the scramjet combustor. In Ref. 6 a solid body drag model was introduced and was used to calculate the trajectory of either a matched pressure or overexpanded jet and the portion of the trajectory downstream of the Mach disk in an underexpanded jet. Recent tests[7–11] of underexpanded jets with both sonic and supersonic injection have provided the data that permits the extension of the previous method to define the complete trajectory of the underexpanded jet. The intent of this paper is to formulate the problem in rather general terms, discuss the limitations of some of the earlier work and present a new unified model of the interaction zone which overcomes the deficiencies of its predecessors.

The general character of the flowfield of an underexpanded sonic or supersonic jet discharging into a supersonic primary flow is depicted in Fig. 1. The principal feature in the secondary jet is the barrel shock structure which terminates in a Mach disk and is followed by a less clearly defined expansion zone. This resembles the structure of an underexpanded jet discharging into a quiescent medium except that the whole secondary flow is partially bent over by the main flow. The structure in the primary flow is essentially that caused by a blunt-body interaction. To render this complex problem tractable, certain assumptions must be made, viz., shear, heat addition, heat transfer, and mixing are neglected in this region. The assumption that no mixing occurs may appear to be overly restrictive, but the subsequent analysis will show that the exchange of normal momentum occurs in the near region of the injector, and both primary and secondary flow are nearly coaxial before substantial mixing occurs. Thus, the solution of the over-all problem of the fuel-air distribution in a scramjet combustor may consist of a solution for the interaction zone to provide the necessary input for a second analysis of a problem of mixing of parallel (but not uniform) streams.

Analysis of the Interaction Problem

To solve the interaction problem, the integral forms of the two sets of the conservation equations are written, one for the primary stream and one for the secondary. Each set of equations includes the scalar energy and continuity equations and the vector momentum equation. If stations in the flow field are chosen wherein the flow properties can be considered to be represented by some suitable average value, then considerable simplicity is introduced in the solution. It is the

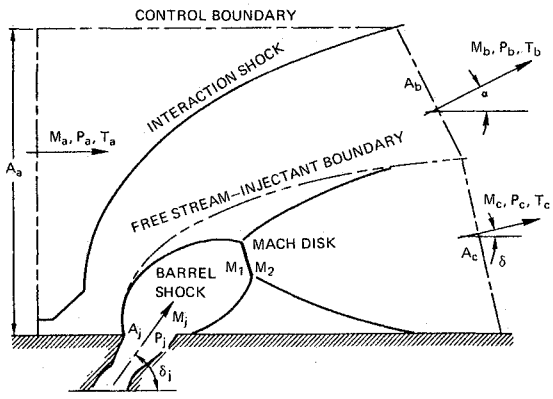

Fig. 1 Generalized model configuration for gaseous secondary injection into a supersonic freestream.

judicious choice of these particular points in the flowfield that enables the success of the subsequent unified analysis. Letting subscripts a and b refer to primary flow conditions across areas A_a and A_b in Fig. 1, and subscripts j and c refer to jet conditions across areas A_j and A_c, the simplified forms of the equations are:

Mass conservation

$$\rho_a u_a A_a = \rho_b u_b A_b \tag{1a}$$

$$\rho_j u_j A_j = \rho_c u_c A_c \tag{1b}$$

Axial momentum conservation

$$p_a A_a - \int_{A_x} p dA - p_b A_b \cos\alpha = \rho_b u_b^2 A_b \cos\alpha - \rho_a u_a^2 A_a \tag{2a}$$

$$p_j A_j \cos\delta_j + \int_{A_x} p dA - p_c A_c \cos\delta = \rho_c u_c^2 A_c \cos\delta - \rho_j u_j^2 A_j \cos\delta_j \tag{2b}$$

Normal momentum conservation

$$-p_\infty \int_{CB} dA + \int_N p dA + \int_{WP} p dA - p_b A_b \sin\alpha = \rho_b u_b^2 A_b \sin\alpha \tag{3a}$$

$$p_j A_j \sin\delta_j - \int_N p dA + \int_{WS} p dA - p_c A_c \sin\delta = \rho_c u_c^2 A_c \sin\delta - \rho_j u_j^2 A_j \sin\delta_j \tag{3b}$$

Energy conservation

$$\rho_a u_a A_a (h_a + u_a^2/2) = \rho_b u_b A_b (h_b + u_b^2/2) \tag{4a}$$

$$\rho_j u_j A_j (h_j + u_j^2/2) = \rho_c u_c A_c (h_c + u_c^2/2) \tag{4b}$$

The sets of equations for the primary flow and the jet are coupled in that the $\int p dA$ terms on the common boundaries of the stream appear in both sets of the momentum equations. Whether or not the two sets of equations must be solved simultaneously depends on the boundary conditions that are assumed. To clarify this point we will examine some of the approaches taken by previous authors to solve this problem. Zukoski and Spaid[2–5] introduced the model shown in Fig. 2a, wherein the effective shape of the injectant is represented as a quarter sphere of radius h followed by an axisymmetric half body. Solutions were obtained at a downstream station in the flow where, in addition to the assumptions made above, it was assumed that the secondary jet had expanded to $p_c = p_b = p_a$. Referring to Fig. 1 and Eqs. (1–4), this model corresponds to $\alpha = \delta = 0°$, $\delta_j = 90°$ and $A_c = \pi h^2/2$. Zukoski and Spaid then made two additional assumptions: 1) the pressure on the quarter sphere due to the primary flow can be calculated by use of modified Newtonian flow, and 2) the injectant expands isentropically to the ambient pressure. However, these two constraints on the problem are contradictory and the solution obtained by arbitrarily

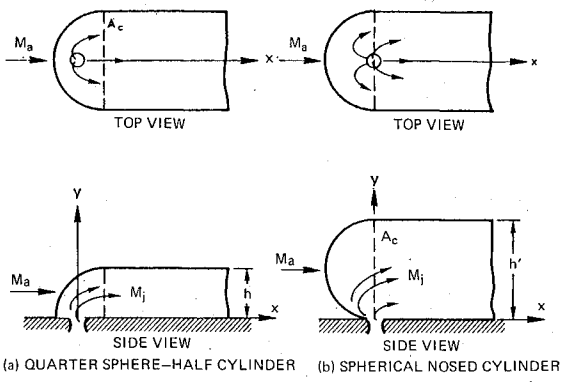

Fig. 2 Models of the effective shape of the injectant causing blunt body interaction in the freestream.

combining intermediate equations from the two cases, i.e.,

$$\left(\frac{2^{1/2}h}{D_j}\right) \equiv \left(\frac{A_c}{A_j}\right)^{1/2} = \frac{1}{M_a}\left[\frac{p_{tj}}{p_a}\frac{\gamma_j}{\gamma_a}\frac{4}{C_p^*}\right]^{1/2} \times \left\{\frac{2}{\gamma_j - 1}\left[\frac{2}{\gamma_j + 1}\right]^{(\gamma_i+1)/(\gamma_i-1)}\left[1 - \left(\frac{p_a}{p_{tj}}\right)^{(\gamma_i-1)/\gamma_i}\right]\right\}^{1/4} \tag{5a}$$

With $\gamma_a = \gamma_j = 1.4$, this becomes

$$\left(\frac{A_c}{A_j}\right)^{1/2} = \frac{2.275}{M_a}\left(\frac{p_{tj}}{p_a C_p^*}\right)^{1/2}\left[1 - \left(\frac{p_a}{p_{tj}}\right)^{2/7}\right]^{1/4} \tag{5b}$$

is mathematically and physically inconsistent. Here D_j is the effective port diameter and thus includes the effect of a discharge coefficient not equal to one which appeared in the original work. Moreover this and many of the following expressions are expressed in terms of $(A_c/A_j)^{1/2}$ to show that the solutions need not be restricted to the particular model shown in Fig. 2a. For example, Eqs. (5a and 5b) would be of the same form for the spherical forebody and cylindrical afterbody with diameter h' shown in Fig. 2b, except $(A_c/A_j)^{1/2} = (h'/D_j)$. The pressure coefficient, C_p^* corresponds to the stagnation pressure behind a normal shock in the primary flow, i.e.,

$$C_p^* = \frac{2}{\gamma_a M_a^2}\left[\left(\frac{\gamma_a + 1}{2}M_a^2\right)^{\gamma_a/(\gamma_a-1)} \times \left(\frac{\gamma_a + 1}{2\gamma_a M_a^2 - \gamma_a + 1}\right)^{1/(\gamma_a-1)} - 1\right] \tag{6a}$$

and for $\gamma_a = 1.4$

$$C_p^* = \left(\frac{8.933M_a^2}{7M_a^2 - 1}\right)^{5/2} - \frac{1}{0.7M_a^2} \tag{6b}$$

Note that in the derivation of Eq. (5a), as well as in the subsequent analysis, the assumption of calorically perfect gases with constant specific heats is made so the simpler relationships would be obtained. Fortuitously, the results from Eq. (5a) adequately describe certain limited experimental observations, which probably explains why a number of subsequent publications have adopted this relationship without rederivation. On the other hand, taken individually, both the Newtonian drag model and the isentropic flow model have some merit and have served as a basis for subsequent refinements by others. For example, in Ref. 12 Newtonian drag over the spherical nosed cylinder (Fig. 2b) was used but the boundary condition $M_c = 1$ instead of $p_c = p_a$ was made. In the subsequent discussion it will be shown that this is in marked disagreement with experimental measurements.

The solution for either case is obtained from Eqs. (1b, 2b, and 4b), using the appropriate expressions for $F_x \equiv \int_{A_x} p dA$, viz;

Newtonian drag model:

$$F_x = A_c p_a (M_a^2 \gamma_a C_p^* + 4)/4 \tag{7a}$$

Isentropic flow model:

$$F_x = p_a A_c \left\{1 + \frac{2\gamma_j}{\gamma_j - 1}\left[\left(\frac{p_{tj}}{p_a}\right)^{(\gamma_i-1)/\gamma_i} - 1\right]\right\} \tag{7b}$$

With these expressions the relationships for $(A_c/A_j)^{1/2}$ are, respectively,

Newtonian Drag Model

$$\left(\frac{A_c}{A_j}\right)^{1/2} = \left(2\frac{p_j}{p_a}\frac{M_j}{M_a}\right)^{1/2}\left(\frac{\gamma_j}{\gamma_a C_p^*}\right)^{1/4} \times \left[\frac{2 + (\gamma_j - 1)M_j^2}{2 + M_a^2\gamma_a C_p^*(\gamma_j - 1)/4\gamma_j}\right]^{1/4} \tag{8a}$$

and Isentropic Flow Model

$$\left(\frac{A_c}{A_j}\right)^{1/2} = \frac{\left[\frac{2}{2 + (\gamma_j - 1)M_j^2}\right]^{(\gamma_i+1)/[4(\gamma_i-1)]}\left(\frac{p_{tj}}{p_a}\right)^{(\gamma_i+1)/(4\gamma_i)}(M_j)^{1/2}}{\left[\frac{2}{\gamma_j - 1}\right]^{1/4}\left[\left(\frac{p_{tj}}{p_a}\right)^{(\gamma_i-1)/\gamma_i} - 1\right]^{1/4}} \tag{8b}$$

For $\gamma_j = 1.4$, and $M_j = 1$, Eq. (8b) yields

$$\left(\frac{A_c}{A_j}\right)^{1/2} = 0.5087\left(\frac{p_{tj}}{p_a}\right)^{3/7}\left[\left(\frac{p_{tj}}{p_a}\right)^{2/7} - 1\right]^{-1/4} \tag{8c}$$

In the subsequent discussion the "effective back pressure" model introduced in Ref. 6 will be expanded to describe in detail the structure of the secondary jet and the interaction with the primary stream. At this point in the discussion, however, only the general character of the model needs to be considered to establish a correspondence with the above simpler models. In this model it is assumed that along the centerline of the jet the flow expands isentropically from the orifice to a Mach disk (See Fig. 1) and is then recompressed by a normal shock to a static pressure $p_{eb} = \frac{2}{3}p_{t'a}$, where $p_{t'a}$ is the Pitot pressure in the primary flow.§ Along other streamlines in the secondary flow in this region the expansion and recompression to p_{eb} is not easily defined; thus, empirically derived expressions for a) the Mach disk location and b) the cross-sectional area distribution are used to obtain the average properties of the flow just downstream of the Mach disk. These expressions, which will be substantiated in the subsequent discussion are, respectively,

$$y_1/D_j^* = M_j^{1/4}(p_j^*/p_{eb})^{1/2} \tag{9}$$

$$\left(\frac{A_1}{A_j}\right)^{1/2} = \frac{r_1}{r_j} = 1 + 1.45\ln\left(\frac{p_j}{p_{eb}}\right)[1 - \exp(-0.322y_1/D_j)] \tag{10}$$

Substituting (9) into (10) and using the continuity expression permits the definition of the average Mach number at station 2, viz.,

$$\bar{M}_2\bar{\Gamma}_2^{1/2} = M_j\Gamma_j^{1/2}(p_j/p_{eb})\left(\frac{D_2}{D_j}\right)^{-2} \tag{11}$$

where

$$D_2/D_j = 1 + 1.45\ln(p_j/p_{eb})\{1 - \exp[-0.322M_j^{1/4}(p_j^*/p_{eb})^{1/2}D_j^*/D_j]\} \tag{12a}$$

§ In Refs. 7 and 9, p_{eb} was set equal to 80% of the static pressure behind a normal shock in the primary flow. Substantiating arguments can be made for either assumption for p_{eb}, but for the most conditions of interest the difference is trivial; e.g., for $\gamma_a = 1.4$ and $1.75 < M_a < 8.6$, the difference is less than 8%.

$$\Gamma_i = 1 + (\gamma_i - 1)M_i^2/2 \quad (12b)$$

$$D_j^*/D_j = M_j^{1/2}[2\Gamma_j/(\gamma_j + 1)]^{(\gamma_i+1)/[4(1-\gamma_i)]} \quad (13a)$$

$$p_j^*/p_j = [2\Gamma_j/(\gamma_j + 1)]^{\gamma_i/(\gamma_i-1)} \quad (13b)$$

and

$$p_2 = p_{eb} = \tfrac{2}{3}p_{t_a}[1 + C_p^*\gamma_a M_a^2/2]\Gamma_a^{\gamma_a/(1-\gamma_a)} \quad (14)$$

Downstream of the Mach disk the flow is assumed to be unidimensional and expands isentropically to $p_c = p_a$. The over-all area ratio is then given by

$$\left(\frac{A_c}{A_j}\right)^{1/2} = \left(\frac{A_c}{A_2}\right)^{1/2}\left(\frac{A_2}{A_j}\right)^{1/2} = \left(\frac{\bar{\Gamma}_c}{\bar{\Gamma}_2}\right)^{(\gamma_j+1)/4(\gamma_j-1)} \times (\bar{M}_2/\bar{M}_c)^{1/2}(D_2/D_j) \quad (15)$$

where

$$\bar{M}_c^2 = [\bar{\Gamma}_2(p_{eb}/p_a)^{(\gamma_j-1)/\gamma_j} - 1]2/(\gamma_j - 1) \quad (16)$$

Solutions for matched-pressure jets (i.e., $p_j = p_{eb}$) and overexpanded jets ($p_j < p_{eb}$) were discussed in detail in Refs. 6 and 11 and therefore will not be included herein. However, it now appears that the assumption of an elliptical cross-sectional area for the jet which is appropriate for very low M_a should be changed to circular for $M_a > 1$. Moreover, low values of p_j relative to p_{eb} are generally not encountered in typical cross stream injection systems.

Before comparing expressions (5, 8, and 15), it is appropriate to determine the minimum and maximum values of $(A_c/A_j)^{1/2}$ consistent with the above constraints. The minimum value of $(A_c/A_j)^{1/2}$ corresponds to the maximum possible value of F_x which would occur if the freestream Pitot pressure $p_{t'a}$ acted on the complete projected area, A_x, which would be equal to A_c if A_c is in contact with the plate, i.e.,

$$F_x \equiv \int_{A_x} p dA = \frac{A_c p_a}{2}(M_a^2\gamma_a C_p^* + 2) \quad (17)$$

$$\left(\frac{A_c}{A_j}\right)_{\min}^{1/2} = \frac{\Gamma_j^{1/4}(p_j M_j/p_a M_a)^{1/2}}{\left(\frac{C_p^*}{2}\frac{\gamma_a}{\gamma_j}\right)^{1/4}\left[1 + \frac{\gamma_j - 1}{2}\left(\frac{\gamma_a M_a^2 C_p^*}{2\gamma_j}\right)\right]^{1/4}} \quad (18)$$

The maximum value of $(A_c/A_j)^{1/2}$ corresponds to a situation wherein the total pressure loss in the secondary jet is also maximum. For inviscid adiabatic flow in the jet and $p_c = p_b = p_a$, the maximum loss would occur if all of the jet expanded isentropically to a pressure $< p_a$ and then recompressed to p_a through a single normal shock; i.e., the normal shock would be located at station c. To obtain this solution the Mach number M_1 ahead of the shock is first obtained from

$$M_1^2 = [(\gamma_j + 1)(p_a/p_{t_j})\,\Gamma_1^{\gamma_i/(\gamma_i-1)} + \gamma_j - 1]/(2\gamma_j) \quad (19)$$

and is then substituted into the isentropic flow relationship

$$(A_c/A_j)^{1/2}_{\max} = (M_j/M_1)^{1/2}(\Gamma_1/\Gamma_j)^{(\gamma_i+1)/4(\gamma_i-1)} \quad (20)$$

Table 1 Downstream properties of flow for various models; $M_a = 2.7$; $M_j = 1.0$, $p_{t_j}/p_{t_a} = 5.0$; $\gamma_a = \gamma_j = 1.4$

Model	$(A_c/A_j)^{1/2}$	M_c	$\frac{\bar{p}}{p_a} = \frac{\int_{A_x} p dA}{p_a A_c}$	$\frac{p_{t_c}}{p_{t_j}}$
Maximum loss	12.97	0.39	1.22	0.01
Zukoski & Spaid	6.41	1.39	3.72	0.03
Newtonian drag	5.43	1.78	5.43	0.05
Effective back pressure	4.51	2.31	8.46	0.11
Maximum $A_x \int p dA$	4.22	2.52	9.86	0.15
Isentropic flow	2.99	3.80	21.25[a]	1.00

[a] Greater than p_{t_a}.

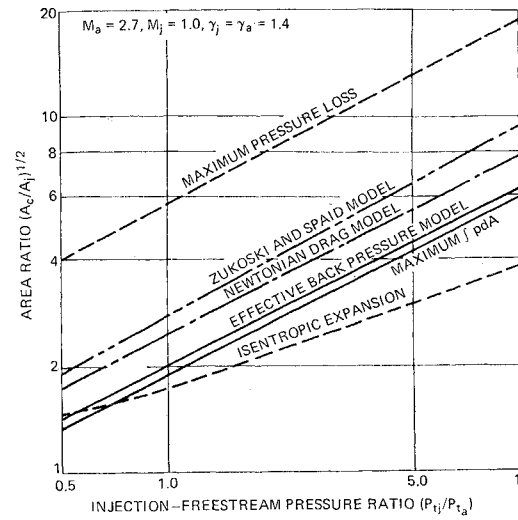

Fig. 3 Comparison of injectant area ratio for various jet penetration models.

Figure 3 compares the results for $(A_c/A_j)^{1/2}$ vs p_{t_j}/p_{t_a} from Eqs. (5, 8, 15, 18 and 20) for the case $M_a = 2.7$, $M_j = 1.0$, $\gamma_a = \gamma_j = 1.4$. The items of particular significance are: 1) the hybrid model of Zukoski and Spaid predicts greater penetration than either of its two genera; 2) the isentropic expansion model violates the condition of maximum F_x at $p_{t_j}/p_{t_a} > 0.75$, thus for higher pressure ratios this model would require A_c to be greater than the projected area; 3) the range of possible values for $(A_c/A_j)^{1/2}$ varies by a factor of 3, and 4) the dependence of $(A_c/A_j)^{1/2}$ on p_{t_j}/p_{t_a} for $p_{t_j}/p_{t_a} > 0.8$ is reasonably well represented for all of the models by $(A_c/A_j)^{1/2} = (p_{t_j}/p_{t_a})^m$ where $m = 0.5$ for all cases except the Maximum Loss ($m = 0.51$) and the Isentropic Flow ($m = 0.33$).

In Table 1 some of the other properties of the flow at station c are given for the particular case of $p_{t_j}/p_{t_a} = 5$. Note that the total pressure recovery in the secondary jet varies from <1% for the maximum loss case to ~15% for the maximum F_x case. The corresponding average pressures on the projected frontal area for the possible solutions vary from 1.22 to 9.86 p_a. Except for the Newtonian drag model (and presumably for a rederived version of the Zukoski and Spaid model) the shape of both the forebody and the section at c have no effect on the other properties at c. The Newtonian-flow results are only applicable for either a quarter-sphere or hemisphere forebody; blunter forebody shapes would have larger F_x and would give results closer to the maximum drag cases; more streamlined shapes would yield larger A_c/A_j.

With F_x defined and $p_b = p_c = p_a$, it is now also possible to find all of the properties in the primary stream at b for a defined α (e.g., $\alpha = 0$) by solving Eqs. (1a, 2a, and 4a). Thus it is apparent that the same set of equations (1a, 2a, 4a, 1b, 2b, and 4b) could have been solved for another specified boundary condition different than $p_b = p_c = p_a$. A particular case of interest is the enclosed duct, the control boundary follows the walls of the duct thus $A_b + A_c$ is known. Wu and Aoyama[13] considered this problem, but instead of using any of the above models they assumed that F_x could be derived from the pressure variation along the *axis* of an underexpanded jet. This model must be a poor one, because the pressure field acting on the jet boundary is dependent on the conditions behind a strong shock in the external flow, and the internal structure of the jet adjusts correspondingly to match this pressure. This can easily be shown in the case of the underexpanded jet discharging into a quiescent medium, wherein the pressure on the jet surface is the external pressure and the centerline pressure decreases monotonically from the

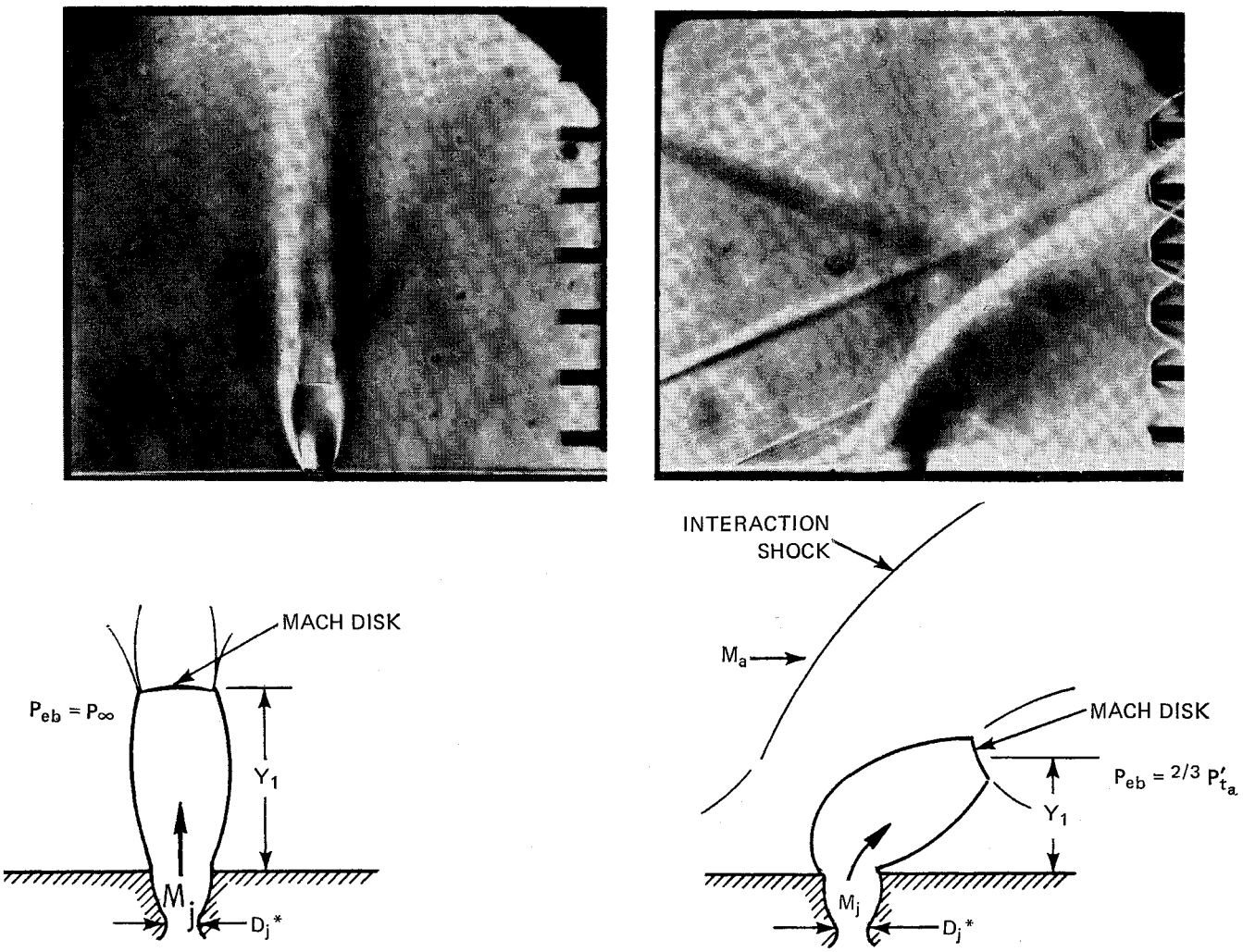

Fig. 4 Shock structure for underexpanded gaseous injection into still air and into a supersonic crossflow.

orifice pressure to a level considerably below the ambient pressure prior to passing through a normal shock.

At this point there is a temptation to relate $(A_c/A_j)^{1/2}$ to some measurable physical dimension of the flowfield. For example, if the semicircular section with radius h of Refs. 2–5 is used, and if it is assumed that the semicircle rests on the surface, then the "dimensionless effective jet height" and the dimensionless center of mass are given by $h/D_j^* = 0.7071\ (A_c/A_j)^{1/2}$, and $\bar{h}/D_j^* = 0.300\ (A_c/A_j)^{1/2}$, respectively. The choice of the semicircular cross section was arbitrary, and experimental measurements (Ref. 4, Fig. 6, and Ref. 11, Fig. 14) indicate that a circular cross section, not necessarily in contact with the surface, is probably more representative. Disregarding this qualification, and assuming contact with the surface, the "effective jet height" would be $h/D_j^* = (A_c/A_j)^{1/2}$, and the center of mass would be $\bar{h}/D_j^* = 0.5\ (A_c/A_j)^{1/2}$. It could be argued, therefore, that favorable correlations with data based on a semicircular section and a model yielding a relatively high $(A_c/A_j)^{1/2}$ may in fact be less justifiable on physical grounds than a similar correlation based on a circular section and model having a lower $(A_c/A_j)^{1/2}$. It is apparent therefore, that by suitable redefinition of the downstream shape a significant change in h/D_j^* or $\bar{h}/D_j^*$ can be obtained and agreement of data could be beneficially affected. This was done in Ref. 14 for the isentropic flow model with the assumption that the downstream shape is the projection of a cone with its small end resting on the surface and with its large end capped with a hemisphere. Errors in the derivation of F_x are, however, present in Ref. 14.

To avoid having to apply such arbitrary constraints to this problem it is necessary to consider in more detail the fine structure of the secondary jet. In Refs. 7, 8, and 11 the similarity of the structure of an underexpanded jet discharging into a quiescent medium and that with crossflow was pointed out. Figure 4 compares schlieren photographs and the corresponding schematic illustrations for a) sonic discharge into still air, and b) sonic discharge into a Mach 2.72 airstream. Although, there is some distortion with crossflow, the same general barrel-shock structure, terminating in a Mach disk, is present. Crist et al.,[15] presented data for sonic injection into a quiescent medium for six different gases with $1.18 \leq \gamma_j \leq 1.67$ and $536 \leq T_{t_j} \leq 7560°R$. Values of y_1/D_j^* from these data have been plotted vs p_j^*/p_∞ in Fig. 5a, where p_∞ is the external pressure. Similar data from Adamson and Nicholls,[16] Love and Grigsby,[17] and new data we have obtained for supersonic injection into a quiescent medium, $1.5 \leq M_j < 3.0$ are plotted vs $M_j^{1/2}p_j^*/p_\infty$ in Fig. 5b. Also shown as a solid line on both figures is the relationship $y_1/D_j^* = M_j^{1/4}(p_j^*/p_\infty)^{1/2}$, which adequately represents the data for both sonic and supersonic injection. More complex expressions for y_1/D_j^* are given by Love and Grigsby[17] for their data, but their expressions do not yield as close agreement with the composite of data shown in Figs. 5a and 5b. By adopting a suitable definition of an effective back pressure, i.e., $p_{eb} = \frac{2}{3}\ p_{t'a}$, it is possible to extend this correlation to the crossflow case. Data from several sources[4,7,9,18] together with data recently obtained by the writers are shown in Fig. 6. Again the correlation $y_1/D_j^* = M_j^{1/4}\ (p_j^*/p_{eb})^{1/2}$ appears to be justified for $1.0 \leq M_j \leq 2.2$

and $1.9 \leq M_a \leq 4.5$. Missing from Fig. 6 are the extensive data from Ref. 10, which includes effects of stagnation temperature and molecular weight, because these data are based on the "top" of the barrel shock rather than the center of the Mach disk. Once the more complete description of the jet structure is explained, a comparison with the latter data will be made.

To obtain the downstream displacement of the Mach disk, x_1, data from the experiments referred to in Fig. 6 were examined. Attempts to correlate these data with several of the important physical parameters were made and the best collapsing of the data was obtained in the plot of x_1/y_1 as a function of M_a/M_j. This correlation is shown in Fig. 7 with the empirical relationship

$$x_1/y_1 = 1.25[1 - \exp(-M_a/M_j)] \tag{21}$$

suitably chosen so as to approximate the data and permit $x_1/y_1 \to 0$ as $M_a \to 0$ as must be the case for discharge into a quiescent medium.

To define the trajectory of the centerline and the angular orientation of the flow at the Mach disk, the trajectory shape is assumed to be parabolic in this region, i.e.,

$$y/D_j^* = [(x/D_j^*)(y_1/D_j^*)/(x_1/y_1)]^{1/2} \tag{22}$$

so that

$$\delta = \arctan[\tfrac{1}{2}(y/D_j^*)/(x/D_j^*)] \tag{23}$$

and from Eq. (21)

$$\delta_1 = \delta_2 = \arctan[0.5/(x_1/y_1)] \tag{24}$$

Downstream of the Mach disk the trajectory of the jet is only weakly dependent on the internal structure of the jet and the concept of the turning of an effective solid body introduced in Ref. 6 can conveniently be used to calculate its shape. The momentum equation normal to the jet centerline is solved (Fig. 8). In differential form this equation can be expressed as:

$$\frac{-mu^2}{R_c} = \rho_j u_j^2 \left(\frac{u}{u_j}\right) d\delta = C_p A_p \rho_a u_a^2/2 \tag{25}$$

where C_p is the averaged pressure coefficient acting on the projected area of the upstream facing surface of the jet. On the downstream surface the pressure is assumed to be equal to p_a, thus $C_p = 0$ on this area. The local pressure coefficient is taken as

$$\tilde{C}_p = C_p^* \sin^2\hat{\delta} \tag{26}$$

where $\hat{\delta} = \delta + \hat{\alpha}$ is the local inclination of the surface and

$$\hat{\alpha} = \arctan\left[\tfrac{1}{2}\frac{d(D/D_j)}{d(s/D_j)}\right] \tag{27}$$

The average value of the pressure coefficient is taken to be the same as the Newtonian about a cylinder, i.e., $C_p = 2\tilde{C}_p/3$. The pressure acts on a projected area

$$A_p = D\left(R_c + \frac{D}{2}\right) d\delta \tag{28}$$

and $ds = dx/\cos\delta = dy/\sin\delta$. These relationships can be substituted into Eq. (25) to yield in dimensionless form

$$d\left(\frac{s}{D_j}\right) = \left[\frac{1}{2}\frac{D}{D_j} - \left(\frac{\tfrac{3}{4}\pi\gamma_j p_j M_j^2}{\gamma_a p_a M_a^2 C_p^*}\right)\frac{(u/u_j)(D_j/D)}{\sin^2\hat{\delta}}\right] d\delta \tag{29}$$

Equation (29) is solved by different methods for the region of flow between the Mach disk and point 3 where the flow has reexpanded to $p = p_a$, and downstream of point 3. In the region between the Mach disk and station 3 it is assumed that the flow expands isentropically from a suitably defined set of conditions at station 2. Even though it is possible to define the streamwise variation in Mach number along

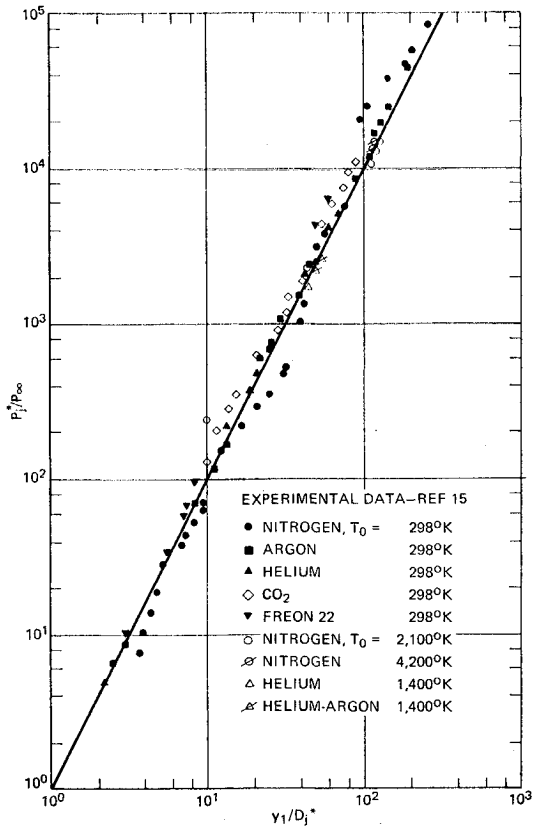

Fig. 5a Correlation of Mach disk height with pressure ratio for sonic injection into a quiescent medium.

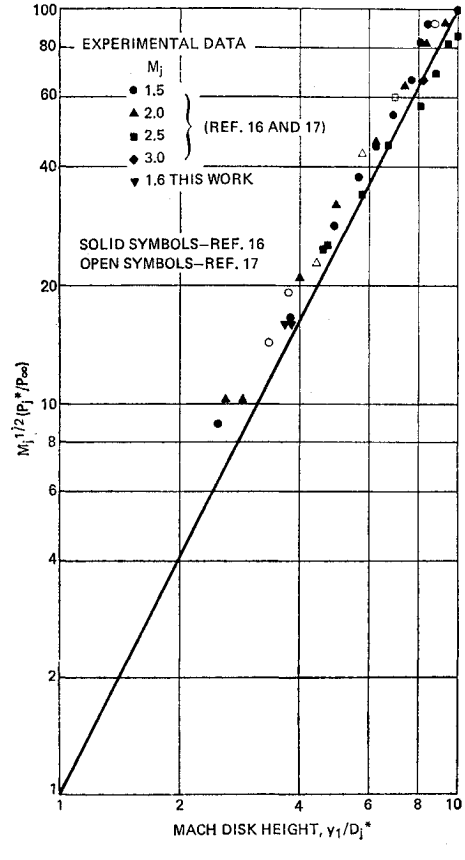

Fig. 5b Correlation of Mach disk height with injection parameters for supersonic injection into a quiescent medium.

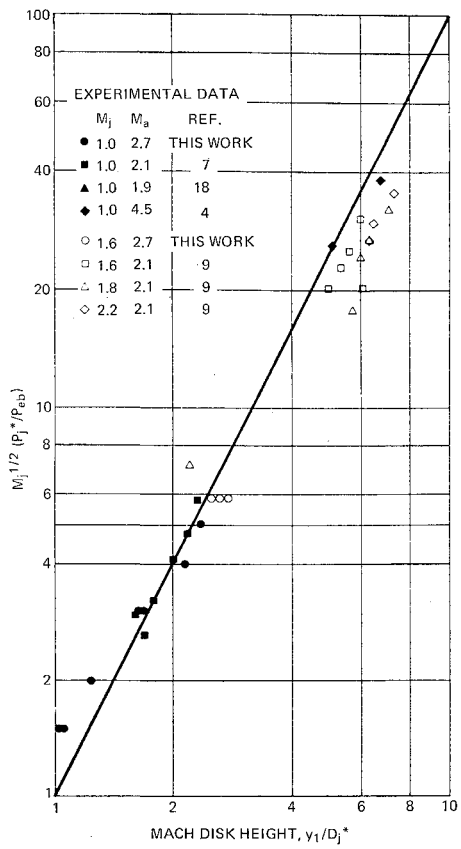

Fig. 6 Correlation of Mach disk height with injection parameters for transverse injection into supersonic flow.

the axis up to the Mach disk and in turn the Mach number just downstream of the normal shock[19] this Mach number is not at all representative of an average condition for station 2. Gradients in flow properties normal to the axis are large and in fact only a portion of the flow passes through the normal shock. Instead the average properties are defined as those corresponding to a one dimensional flow with $\bar{p}_2 = p_{eb}$ and $A_2 = A_1$ defined by Eq. (10). Area was chosen because both experimental data and theoretical methods for obtaining the jet boundary of a jet discharging into a quiescent medium are available. The same variation is assumed to be valid with external flow present. A comparison of the more general expression

$$\left(\frac{A}{A_j}\right)^{1/2} = \frac{r}{r_j} = 1 + 1.45 \ln\left(\frac{p_j}{p_\infty}\right)[1 - \exp(-0.322\, y/D_j)] \tag{30}$$

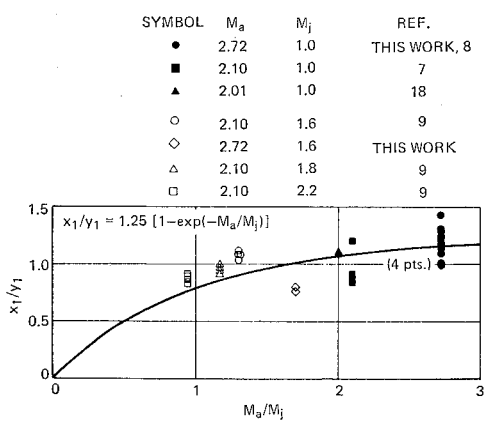

Fig. 7 Correlation of the coordinates of the center of the Mach disk with Mach number ratio.

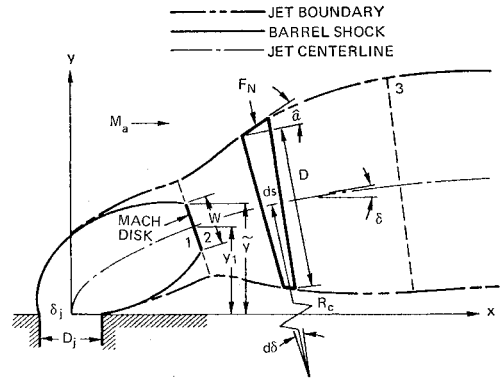

Fig. 8 Model for jet centerline trajectory calculation.

with solutions obtained by the method of characteristics by Love and Grigsby[17] are shown in Fig. 9. The boundaries for various M_j tend to collapse to a single curve for each p_j/p_∞ when the coordinates are normalized to r_j, and Eq. (30) is in reasonable agreement considering the wide range of $p_j{}^*(2 \leq p_j{}^*/p_\infty \leq 388)$ that is covered. With A_2 defined by Eq. (10) and $\bar{M}_2$ by Eq. (11), all other average properties at 2 can be found; e.g.,

$$\bar{u}_2/u_j = (\Gamma_j/\bar{\Gamma}_2)^{1/2}\bar{M}_2/M_j \tag{31}$$

In region 2–3 increments in p/p_a between p_{eb}/p_a and 1 are selected and the isentropic flow equations are used to find the corresponding values of $\bar{M}$, $\bar{u}/\bar{u}_j$ and $\bar{D}/D_j$, i.e.,

$$\bar{M}^2 = 2\left\{\left[\frac{p_{eb}}{p_a}\frac{p_a}{\bar{p}}\right]^{(\gamma_i-1)/\gamma_i}\bar{\Gamma}_2 - 1\right\}\Big/(\gamma_j - 1) \tag{32}$$

$$\bar{u}/u_j = (\Gamma_j/\bar{\Gamma}_M)^{1/2}\bar{M}/M_j \tag{33}$$

$$\frac{\bar{D}}{D_j} = \frac{\bar{D}_2}{D_j}\left(\frac{\bar{M}_2}{\bar{M}}\right)^{1/2}\left(\frac{\bar{\Gamma}_M}{\bar{\Gamma}_2}\right)^{(\gamma_i+1)/4(\gamma_i-1)} \tag{34}$$

To integrate Eq. (29) it is necessary to relate D to s so the jet shape correlation used upstream of the Mach disk is again assumed to be valid, if the initial conditions are taken to be the average conditions at 2 and the axial coordinate is taken

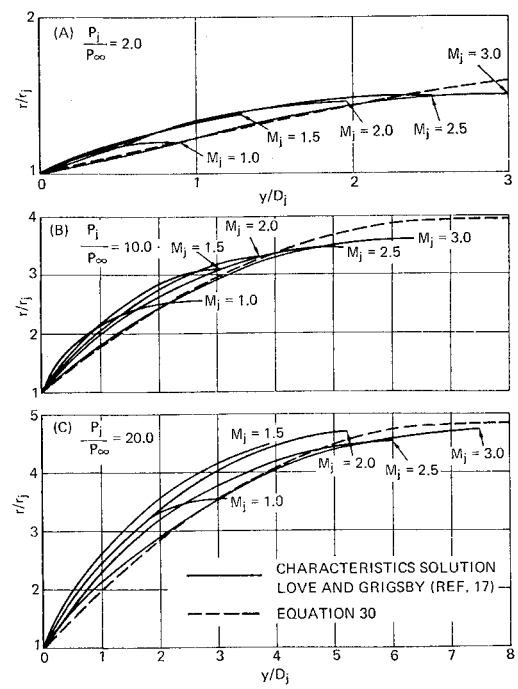

Fig. 9 Comparison of calculated jet boundaries for injection into a quiescent medium.

as $s - s_2$, i.e.,

$$\frac{\bar{D}}{D_j} = \frac{\bar{D}_2}{D_j}\{1 + 1.45\ln(p_{eb}/p_a)[1 - \exp(-0.322 [s - s_2]/\bar{D}_2)]\} \quad (35)$$

The integration is performed by first differentiating Eqs. (32), (34) and (35) analytically and combining with Eq. (29), i.e., taking

$$\frac{d(s/D_j)}{d(\bar{p}/p_a)} = \frac{d(s/D_j)}{d(\bar{D}/D_j)} \cdot \frac{d(\bar{D}/D_j)}{d(\bar{M})} \cdot \frac{d(\bar{M})}{d(\bar{p}/p_a)} \quad (36a)$$

thus defining

$$f(\bar{p}/p_a,\bar{\delta}) = \frac{d(\bar{\delta})}{d(\bar{p}/p_a)} = \frac{d(\bar{\delta})}{d(s/D_j)} \frac{d(s/D_j)}{d(\bar{p}/p_a)} \quad (36b)$$

to give

$$(\bar{\delta} - \delta_2) = \int_{p_{eb}/p_a}^{\bar{p}/p_a} \frac{f\bar{p}}{p_a,\bar{\delta}} \frac{d(\bar{p})}{p_a} \quad (37)$$

and

$$(x - x_2)/D_2 = \int_{p_{eb}/p_a}^{\bar{p}/p_a} \cos\bar{\delta} \left[\frac{d(s/D_j)}{d(\bar{p}/p_a)}\right] d(\bar{p}/p_a) \quad (38)$$

$$(y - y_2)/D_2 = \int_{p_{eb}/p_a}^{\bar{p}/p_a} \sin\bar{\delta} \left[\frac{d(s/D_j)}{d(\bar{p}/p_a)}\right] d(\bar{p}/p_a) \quad (39)$$

Equation (37) was integrated numerically with a third-order Runge-Kutta method, and the values of $\bar{\delta}$ so calculated were fed into a concurrent Simpson's Rule integration of Eqs. (38 and 39).

In the region downstream of 3 the flow properties within the jet remain constant while the stream continues to turn toward $\delta = 0$. In this region, $d = d_3$, $u = u_3$ and $\hat{\delta} = \delta$, thus Eq. (29) can be integrated in closed form to yield

$$\frac{y - y_3}{D_j} = K \ln\left[\frac{\tan\delta/2}{\tan\bar{\delta}_3/2}\right] - \tfrac{1}{2}\frac{\bar{D}_3}{\bar{D}_j}(\cos\bar{\delta} - \cos\bar{\delta}_3) \quad (40)$$

and

$$\frac{x - x_3}{D_j} = \left[\frac{\bar{D}_3}{2D_j}(\sin\bar{\delta} - \sin\bar{\delta}_3) - \frac{K}{\sin\bar{\delta}} + \frac{K}{\sin\bar{\delta}_3}\right] \quad (41)$$

where

$$K = \frac{-\frac{3}{4}\pi\left(\frac{\bar{u}_3}{u_j}\right)\left(\frac{D_j}{\bar{D}_3}\right)\left(\frac{\gamma_j}{\gamma_a}\right)\left(\frac{p_j}{p_a}\right)\left(\frac{M_j}{M_a}\right)^2}{C_p^*} \quad (42)$$

Although this calculation could be continued to $\delta = 0$, some reasonable limitation should be set, e.g., $x/D_j \leq 10$, because the effects of essentially coaxial turbulent mixing would become appreciable and should therefore be included in the analysis. The jet trajectory is now completely defined, thus parametric studies and comparisons with experimental results can now be made. First let us examine the solutions for the cases previously covered by the simpler analysis and summarized in Fig. 3 and Table 1 for $M_a = 2.7$.

Trajectories for these cases are shown in Fig. 10 for $p_{tj}/p_{ta} = 1$, 2, 5, and 10. The centerline trajectories turn over within a few diameters downstream of the injector and are approaching the horizontal at $x/D_j^* = 10$. Figure 10b shows similar sets of trajectories for $M_j = 2$. For the same p_{tj}/p_{ta}, increasing M_j steepens the trajectory and results in slightly increased penetration. Note that the $p_{tj}/p_{ta} = 1, 2$; $M_j = 2$ cases are slightly underexpanded but are included for completeness. In Fig. 11 the $M_j = 1$ results are replotted on a scale normalized such that cases for $p_{tj}/p_{ta} > 1$, would have mass flow equal to the case of $p_{tj}/p_{ta} = 1$, i.e., $D_j^* \sim (p_{tj}/p_{ta})^{-1/2}$. This comparison shows that varying injection pressure but holding mass flow constant

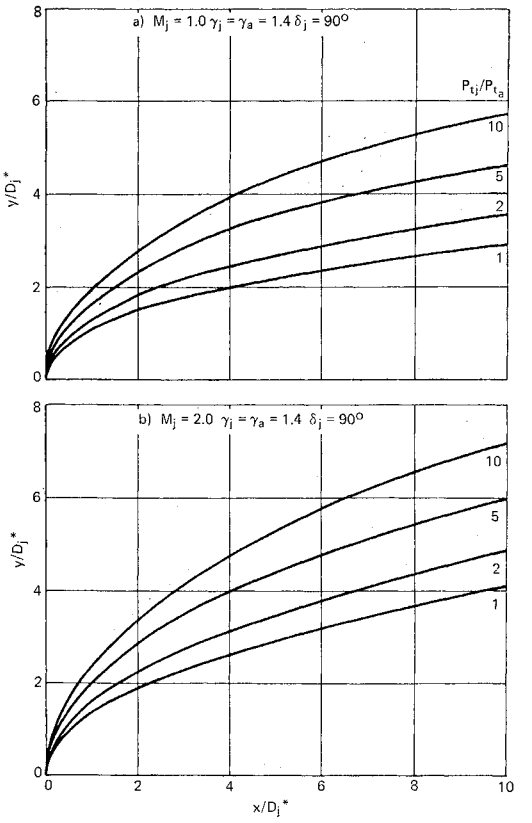

Fig. 10 Comparison of jet trajectories showing the effects of variation in injectant Mach number and injectant/freestream pressure ratio, $M_a = 2.7$.

has very little effect on the absolute penetration of the secondary jet. Similar conclusions were reached in Ref. 11.

The typical constraint encountered in combustor design is that of constant mass flux ratio, i.e., $\rho_j u_j/\rho_a u_a$ = constant with varying M_a. This effect is examined in Fig. 12 wherein $M_j = 1$, $\gamma_j = \gamma_a = 1.4$ and p_{tj}/p_{ta} was varied from 27.58 at $M_a = 1.5$ to 10 at $M_a = 2.7$ and 1.30 at $M_a = 5$ to hold the mass flux ratio constant. Centerline trajectories are only weakly dependent on M_a with somewhat better penetration at lower M_a values.

Comparisons with Experimental Results

Figure 13 shows the calculated centerline trajectory and Mach disk location for sonic hydrogen injection into a Mach 2.7 airstream with $p_{tj}/p_{ta} = 1.6$. The calculated edge of the one-dimensional jet is obtained by adding and subtracting a distance $\frac{1}{2}D/D_j$ normal to the local jet center. These results are compared with the experimentally observed Mach disk, the maximum and median H_2 (half of the hydrogen lies inside a circle through these points) concentration at $x/D_j^* = 5$ and 10, and the center of mass flux and line of zero H_2 concentration at the same locations. The experimental apparatus used in these tests is described in detail in Ref. 11. The edge of the one-dimensional jet should be representative of the extent of the median H_2 concentration profile. The data points were obtained from detailed pitot pressure, cone-static pressure, and gas-sampling measurements, which were used to deduce the local pressure, temperature, velocity, and H_2 concentration. Contours of constant H_2 concentration, mass flux per unit area, Mach number etc. were made and integrations performed to locate the circle containing one half of the hydrogen mass and mass averaged values of Mach number, total pressure etc.

Figure 14 compares concentration contours measured at $x/D_j^* = 5$, (left side) with the one-dimensional jet bounda-

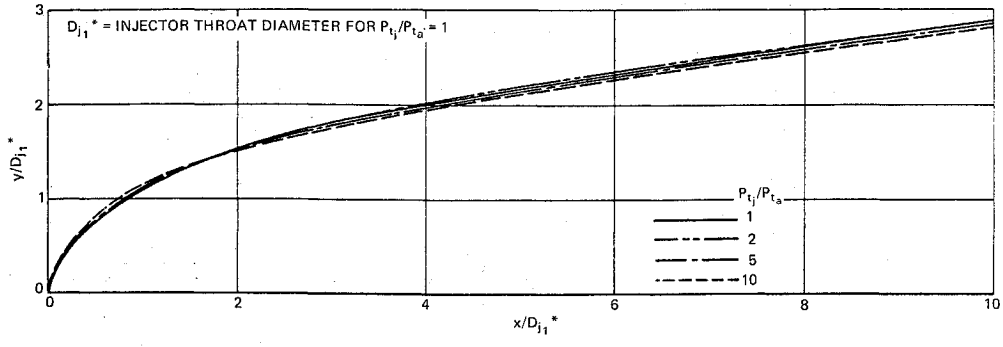

Fig. 11 Comparison of jet trajectories for sonic jets of equal mass flow in a Mach 2.7 freestream.

ries predicted from this analysis and that of Refs. 2–5 (right side). The outer edge (predicted median H_2 concentration) from the Zukoski and Spaid model extends (at $z/D_j^* = 0$) only to the predicted center of the jet for the present model, which, in turn, corresponds to the point of maximum H_2 concentration. Moreover, the experimental contours confirm that 1) a circular section rather than a semicircular section is more representative of the jet shape and 2) the jet centerline lies significantly above the point which would put the jet boundary (i.e., the lower edge for mediam H_2 concentration in contact with the surface. If this effect were to be properly accounted for in the simpler models originally discussed, it would be necessary to place the centroid at station c on the jet centerline. For all cases except the maximum pressure loss case, this would result in an increased frontal area and thus reduce the required average pressure acting on the projected area. For example, the value of $\bar{p}/p_a$ in Table 1 for the "effective-back-pressure" model would decrease from 8.46 to 5.40 assuming $\delta_c \approx 0$ at $x/D_j^* = 10$. At $x/D_j^* = 5$ and $z/D_j^* = 0$, the outer edge of the median H_2 concentration contour is at $y/D_j^* = 4.2$, whereas the $X_{H_2} = 0.5$ contour crosses the $z/D_j^* = 0$ axis at $y/D_j^* = 4.7$ and the theoretical contour is at $y/D^* = 3.9$. The mass averaged one-dimensional Mach number at $x/D_j^* = 5$ computed from the theoretical analysis is 2.336 compared to the mass averaged experimental value of 2.2 and the value corresponding to the Zukoski and Spaid model is 1.47.

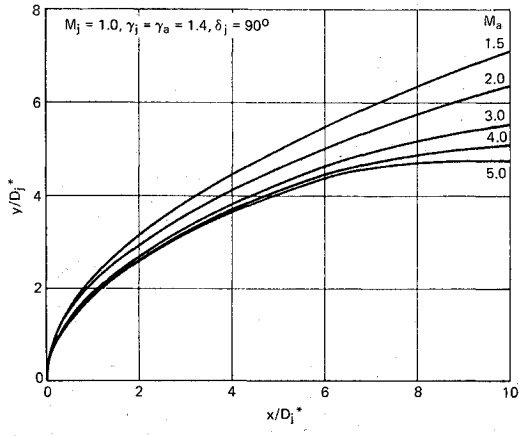

Fig. 12 Comparison of jet trajectories showing the effects of variation in M_a with constant mass flux ratio.

Experimental concentration profiles from Ref. 4 for a case of argon injection into a Mach 2.56 airstream at $x/D_j = 11.1$ are compared with the predicted one-dimensional profiles in Fig. 15. The features of this comparison are similar to those noted for Fig. 14. Equally good comparisons of the present theory with other data given in Refs. 4, 8, and 11 have been made.

In order to compare this theoretical procedure with the other type of information given in the literature, viz., the top of the barrel shock in the initial expansion, it is necessary to define another physical characteristic of the barrel-shock structure. The ordinate of the top of the barrel shock (Figs. 4 and 8) is nearly the same as that of the farthest outboard point on the Mach disk. Thus, adding $\cos\delta_2 W/2$ to the ordinate of the center of the Mach disk gives an approximation of this point. To express W in terms of the injection and primary stream parameters, the experimental results of Ref. 19 with jets discharging into a quiescent medium are used. The expression

$$W/D_j = 3.6[1 - 1.07 \exp(-0.07 p_j/p_\infty)] \qquad (43)$$

adequately approximates the data for $1 \leq M_j \leq 3$ and $0 \leq p_j/p_\infty \leq 54$ as shown in Fig. 16. With crossflow the same expression is assumed valid when p_{eb} is substituted for p_∞. The maximum ordinate of the Mach disk, $\bar{y}$ can be obtained

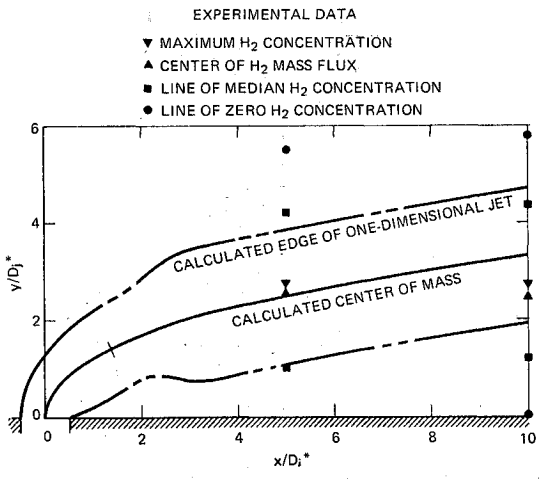

Fig. 13 Comparison of unified jet penetration model with experimental measurements from H_2-air penetration tests with $M_a = 2.7$; $M_j = 1.0$; $p_{t_j}/p_{t_a} = 1.6$; $\delta_j = 90°$.

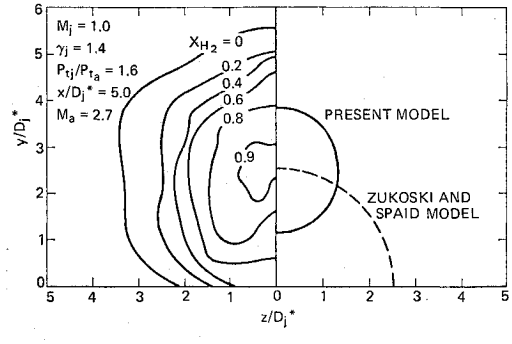

Fig. 14 Comparison of calculated jet cross-sectional areas and measured jet concentration contours (mole fraction) for H_2-air injection.

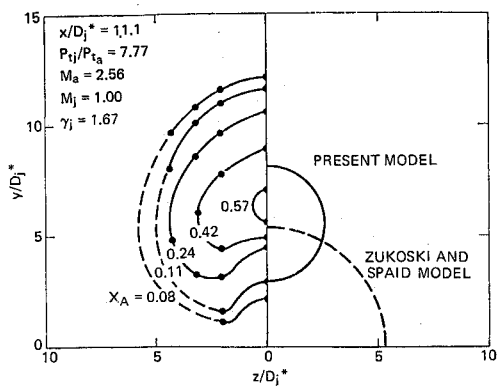

Fig. 15 Comparison of calculated jet cross-sectional areas, and measured jet concentration contours (mole fraction) for argon-air injection (Ref. 3).

from Eqs. (9, 21, 24, and 43), i.e.,

$$\frac{\tilde{y}}{D_j^*} \approx M_j^{1/4}\left(\frac{p_j^*}{p_{e_j}}\right)^{1/2} + \frac{1.8[1 - 1.07\exp(-0.07p_j/p_{eb})]}{\{1 + 0.16[1 - \exp(-M_a/M_j)]^{-2}\}^{1/2}}\left(\frac{D_j}{D_j^*}\right) \quad (44)$$

Figure 17 is a replot of the data which appeared as Fig. 4 in Ref. 10. These tests were made with sonic injection of nitrogen into a Mach 2.8 airstream. Added to the figure are the theoretical curves given by Eq. (44) and the value of h/D_j^* from the Zukoski and Spaid Model. Equally good correlations of Eq. (44) with data from helium and argon injection into air presented in Ref. 10 were obtained. Although physically there is no justification for relating the diameter of the half cylinder or full cylindrical body to this particular point on the barrel shock structure, it is of interest to note that the value of h from the original work of Zukoski and Spaid is also in general agreement with the data. Moreover, if in the development of this theory only the Newtonian Drag Assumption had been made the agreement would even be better.

Concluding Remarks

In conclusion it should be re-emphasized that the validity of this model rests on premise that a similarity exists between the structure of an underexpanded jet discharging into a crossflow and that of a jet discharging into a quiescent medium. The critical parameter needed for this analogy is an "effective back pressure." Empirical relationships which describe the general characteristics of the structure of the jet in the quiescent medium were obtained and were used for the case with crossflow. Uncorrelated experimental and theoretical values could have been used but only with considerably greater computational effort, which considering the approximate nature of the analysis, would not have been warranted. A PL/I (IBM 360) computer program was developed for complete numerical computation of the trajectories, but considerable information regarding the general character of the jet can be readily obtained from Eqs. (9 and 21) for the coordinates of the Mach disk, Eq. (24) for the angular orientation of the flow at the Mach disk, Eq. (44) for the ordinate of the top of the Mach disk and Eq. (15) for the diameter of the jet after expansion to p_a. The complete computer program is available from the authors for those who wish to experiment with the model.

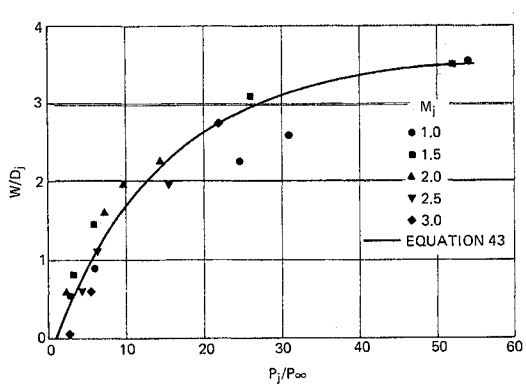

Fig. 16 Correlation of Mach disk width based on experimental measurements of Love and Grigsby (Ref. 17).

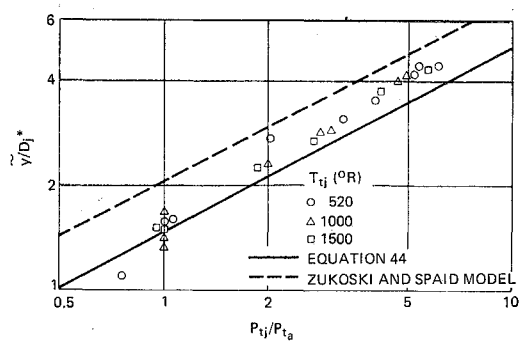

Fig. 17 Comparison of calculated values of the maximum ordinate of the Mach disk and values measured by Chrans and Collins (Ref. 10).

References

[1] Walker, R. E., Stone, A. R., and Shandor, M., "Secondary Gas Injection in a Conical Rocket Nozzle," *AIAA Journal*, Vol. 1, No. 2, Feb. 1963, pp. 334–338.

[2] Zukoski, E. E. and Spaid, F. W., "Injection of Gases into a Supersonic Flow," NASA contract 7-100, Oct. 1963, Guggenheim Jet Propulsion Center, California Institute of Technology, Pasadena, Calif.

[3] Zukoski, E. E. and Spaid, F. W., "Secondary Injection of Gases into a Supersonic Flow," Solid Propellant Rocket Conference, Palo Alto, Calif., 1964.

[4] Zukoski, E. E. and Spaid, F. W., "Secondary Injection of Gases into a Supersonic Flow," *AIAA Journal*, Vol. 2, No. 10, Oct. 1964, pp. 1689–1696.

[5] Spaid, F. W., Zukoski, E. E., and Rosen, R., "A Study of Secondary Injection of Gases into a Supersonic Flow," NASA TR 32-834, Aug. 1966, California Institute of Technology, Pasadena, Calif.

[6] Schetz, J. A. and Billig, F. S., "Penetration of Gaseous Jets Injected into a Supersonic Stream," *Journal of Spacecraft and Rockets*, Vol. 3, No. 11, Nov. 1966, pp. 1658–1665.

[7] Schetz, J. A., Hawkins, P. F., and Lehman, H., "Structure of Highly Underexpanded Transverse Jets in a Supersonic Stream," *AIAA Journal*, Vol. 5, No. 5, May 1967, pp. 882–884.

[8] Orth, R. C. and Funk, J. A., "An Experimental and Comparative Study of Jet Penetration in Supersonic Flow," *Journal of Spacecraft and Rockets*, Vol. 4, No. 9, Sept. 1967, pp. 1236–1242.

[9] Schetz, J. A., Weinraub, R. A., and Mahaffey, Jr., R. E., "Supersonic Transverse Injection into a Supersonic Stream," *AIAA Journal*, Vol. 6, No. 5, May 1968, pp. 933–934.

[10] Chrans, L. J. and Collins, D. G., "Effect of Stagnation Temperature and Molecular Weight Variation of Gaseous Injection into a Supersonic Stream," *AIAA Journal*, Vol. 8, No. 2, Feb. 1970, pp. 287–293.

[11] Orth, R. C., Schetz, J. A., and Billig, F. S., "The Interaction and Penetration of Gaseous Jets in Supersonic Flow," CR-1386, July 1969, NASA.

[12] Cassel, L. A., Davis, J. G., and Engh, D. P., "Lateral Jet Control Effectiveness Prediction for Axisymmetric Missile Configurations—Final Report," Rept. RD-TR-68-5, June 1968, U.S. Army Missile Command, Redstone Arsenal, Ala.

[13] Wu, J. M. and Aoyama, K., "Analysis of Transverse Secondary Injection Penetration into Confined Supersonic Flow," AIAA Paper 69-2, New York, 1969.

[14] Wilson, W. G. and Comparin, R. A., "An Analysis of the Flow Disturbance and Side Forces Due to Gaseous Secondary

Injection into a Rocket Nozzle," AIAA Paper 69-443, Colorado Springs, Colo., 1969.

[15] Crist, S., Sherman, P. M., and Glass, D. R., "Study of the Highly Under-expanded Sonic Jet," *AIAA Journal*, Vol. 4, No. 1, Jan. 1966, pp. 68–71.

[16] Adamson, Jr., T. C. and Nicholls, J. A., "On the Structure of Jets from Highly Underexpanded Nozzles into Still Air," *Journal of the Aerospace Sciences*, Vol. 26, No. 1, 1959, pp. 16–24.

[17] Love, E. S. and Grigsby, C. E., "Some Studies of Axisymmetric Free Jets Exhausting from Sonic and Supersonic Nozzles into Still Air and into Supersonic Streams," RM L54L31, 1955' NACA.

[18] Morkovin, M. V., Pierce, C. A., and Craven, C. E., "Interaction of a Side Jet with a Supersonic Main Stream," Bulletin 35, 1952, Univ. of Michigan, Engineering Research Institute, Ann Arbor, Mich.

[19] Owen, P. L. and Thornhill, C. K., "The Flow in an Axially-Symmetric Supersonic Jet from a Nearly Sonic Orifice into a Vacuum," R and M 2616, 1952, British Aeronautical Research Council.

JUNE 1971 AIAA JOURNAL VOL. 9, NO. 6

Acoustic Characteristics of a High-Subsonic Jet

L. MAESTRELLO* AND E. MCDAID†
NASA Langley Research Center, Hampton, Va.

The acoustic source regions of a subsonic cold jet were traced as far as the periphery of the jet by means of the pressure field on a plane rigid surface located in the vicinity of the jet. The centers of these regions were determined to be from 4 to 18 diam downstream of the exit. Additional measurements were made of flow variables within the jet. From these measurements, the downstream kinetic energy dissipation rate was calculated. Finally, the acoustic radiation characteristics of several simple nozzle configurations were measured. Results indicate that, although considerable alternating of directivity and spectral content of the noise result from varying nozzle geometry, only limited reductions in total sound power resulted.

Introduction

THE general format for nearly all recent work in aerodynamic noise was established by Lighthill[1,2] when he related the sound pressure generated by turbulence to a system of equivalent quadrupole sources in a medium at rest. An alternate approach, mathematically equivalent to Lighthill's but using simple sources, was developed by Ribner.[3] Initial application of the Lighthill theory was made by Proudman,[4] who determined the sound pressure generated by isotropic turbulence. Lilley[5] first used the classification "self noise" and "shear noise" of jets to separate the high-frequency noise due to turbulence-turbulence interaction from the low-frequency noise due to turbulence-shear interaction. The effects of convection were discussed by Ffowcs Williams[6] as well as by Jones.[7] Application of the theory to the radiation of sound in the presence of surfaces was done by Curle,[8] Powell,[9] Lyamshev,[10] and Ffowcs Williams.[11] Acoustic aspects of combustion instability were reported by Kandratiev and Rimski-Korsakov.[12] The distribution of acoustic sources in the jet was determined by Ribner[13] and Powell[14] using similarity considerations and Lighthill's U^8 law. Ribner[15] recently showed that for a low-speed jet, only nine of the possible 36 distinct quadrupole correlations yield distinct nonvanishing contributions to the sound power.

The present paper introduces an experimental technique to locate the acoustic source regions of a jet. In addition, acoustic measurements were made of changes in directivity, spectral content, and total sound power due to changes in nozzle geometry.

Presented as Paper 70-234 at the AIAA 8th Aerospace Sciences Meeting, New York, January 19–21, 1970; submitted February 9, 1970; revision received November 23, 1970. The authors wish to express thanks to J. E. Ffowcs Williams for his helpful discussions and T. Clark for his technical assistance.

* Aero-Space Technologist, Acoustic Branch. Member AIAA.
† Aero-Space Technologist, Acoustic Branch.

Distribution of Sound Sources in a Jet

Lighthill formulated the aerodynamic noise problem using an acoustic analogy. In this model, the fluid turbulence giving rise to sound generation and scattering are replaced by an equivalent distribution of acoustic quadrupole sources in a medium at rest. Mathematically, the model appears as the following nonhomogeneous wave equation

$$\partial^2\rho/\partial t^2 - a_0^2\nabla\rho^2 = \partial^2 T_{ij}/\partial x_i \partial x_j$$

where $T_{ij} = \rho v_i v_j - \tau_{ij} + (p - a_0^2\rho)\delta_{ij}$, a_0^2 is the local speed of sound, ρ is the density, v_i is a component of velocity, τ_{ij} is the viscous stress, and p is the thermodynamic pressure.

In the absence of surfaces, this wave equation can be replaced by the following integral equation for points $\mathbf{x}$ in the far field

$$\Delta\rho(\mathbf{x},t) = \frac{x_i x_j}{4\pi a_0^4 |\mathbf{x}|^3} \int \frac{\partial^2 T_{ij}\mathbf{y}, t - |\mathbf{x} - \mathbf{y}|/a_0}{\partial t^2}\, d^3|\mathbf{y}|$$

where $\Delta\rho(\mathbf{x},t) = \rho(\mathbf{x},t) - \rho_0$, and ρ_0 is the density of the acoustic medium at rest.

The autocorrelation of the far-field density fluctuation can be written as

$$R(\mathbf{x},\tau) = \frac{x_i x_j x_l x_m}{16\pi^2 a_0^8 |\mathbf{x}|^6} \iint \frac{\partial^4}{\partial \tau_0^4} R_{ijlm}(\mathbf{y},\mathbf{y}',\tau_0) d^3|\mathbf{y}| d^3|\mathbf{y}'|$$

where

$$R_{ijlm}(\mathbf{y},\mathbf{y}',\tau_0) = \overline{T_{ij}(\mathbf{y},\tau') T_{lm}(\mathbf{y}',\tau' + \tau_0)}$$

$$\tau' = t - |\mathbf{x} - \mathbf{y}|/a_0,\ \tau_0 = \tau - (|\mathbf{x} - \mathbf{y}'| - |\mathbf{x} - \mathbf{y}|)/a_0$$

Efforts to determine the acoustic source locations in a jet have centered around the determination of the tensor R_{ijlm}.[16]

An alternate approach has been used in the present investigation. Instead of actually measuring R_{ijlm} within the jet, measurements of the sound field near the jet have been